Landscape Architecture

ARTICLE

Hydrothermal Performance of Partial Photovoltaic Shading on a Sedum Green Roof

Nigel Dunnett* **and James William**

The University of Sheffield

* Correspondence: n.dunnett@sheffield.ac.uk

Abstract

In photovoltaic green roofs, the electricity generation takes place over the vegetated surface via solar-electric process, whereas the thermal behavior is governed by evapotranspiration, substrate heat storage, and vegetation exposure under the effect of solar radiation. In the following section, a measured data set of sedum green roof in Ljubljana with elevated photovoltaics will be analyzed based on the comparison of three shade conditions of the vegetation surface: unshaded, partially shaded, and fully shaded. The Hydrothermal Constraint Number depends on evapotranspiration similarity, the vegetation-temperature correlation adjusted according to shading, photovoltaics' correction to the evapotranspiration in the longwave range, and daytime heat-flux fraction to the heat flux reference. The measured evapotranspiration rate for 9 July 2024 is 3.98 mm day^{-1}, and the modeled value is 4.15 mm day^{-1}; for 25 July 2024, they are 4.08 mm day^{-1} and 3.95 mm day^{-1}; and for 3 August 2024, they are 2.60 mm day^{-1} and 2.73 mm day^{-1}. Thus, the corresponding RMSE is 0.145 mm day^{-1}, the mean absolute error is 4.15 %, and the fidelity coefficient is 0.959. The vegetation-temperature correlation, $\theta_v = 0.935\theta_a + 0.011R_g(1 - S)$, implies that every reduction of the short-wave shade-sensitive irradiation by 100 W m^{-2} results in the decrease of the solar thermal component of approximately 1.1 °C. Photovoltaics correction to the evapotranspiration by the long-wave exchange leads to the change in evapotranspiration.

Keywords: photovoltaic green roof; sedum roof; evapotranspiration; module shade; longwave radiation; soil heat flux; roof microclimate; Hydrothermal Constraint Number

1. Introduction

Urban roofs are becoming more active environmental surfaces. On one hand, photovoltaic panels produce electrical energy. On the other hand, roof vegetation retains precipitation, minimizes roof-surface warming, and supports evaporation-driven cooling. If photovoltaics and roof vegetation coexist, there is interaction between the module and the vegetation through radiation effects, heat storage, water vapour transport, and substrate moisture content. The module blocks direct solar irradiation, decreases the visible sky above the vegetation canopy, forms a long-wave radiant surface, and alters the pattern of heating of the substrate. Vegetation and the substrate under it affect near-module temperature and humidity. Consequently, a photovoltaic green roof needs to be assessed in terms of the coupling between the module, vegetation, substrate, drainage system, and roof micro-climate.

Green roof literature is a primary source for the physical framework. Extensive roofs reduce roof-surface heating,

Received: 10 December 2024; Revised: 10 March 2025; Accepted: 19 May 2025; Published: 30 September 2025.

doi: 10.70517/la20251153-05

delay runoff, and provide ecological benefits under conditions of proper selection of plant species, substrate depth, drainage, and irrigation [4, 12, 21]. Literature on hydrology shows that retention and water quality depend on substrate depth, rainfall pattern, season, type of vegetation, age of the roof, and substrate moisture rather than on greening itself [5, 17]. Similarly, literature on energy demonstrates that the effectiveness of a green roof in terms of energy relies on radiation exchange, substrate moisture, degree of coverage with vegetation, and thermal storage within the assembly [6, 7, 13, 25]. All these findings apply to the analysis of photovoltaic green roofs since the module modifies the conditions of radiation and moisture affecting performance of green roofs.

Evapotranspiration connects thermal and hydrological processes of the roof. Evapotranspiration removes heat energy in form of latent heat flux and determines the daily water balance of the substrate (supply, storage, loss). Evapotranspiration theory in classical terms establishes a relationship between radiation, vapor pressure deficit, aerodynamics, and surface resistance [3, 18, 23]. The characteristics of roof environments, however, differ from those of field environments (small depth, heterogeneity, specific wind fields caused by the buildings, interruptions by parapets, services, drains, etc.). For that reason, green-roof studies highlight the need to interpret evapotranspiration with uncertainty and roof-specific context in mind [10, 14, 28]. This paper follows this approach by using three daily pairs of measured and modelled values of evapotranspiration as an indicator of reliability.

Vegetation response is the second component of control. Sedum-based extensive roofs are commonly selected due to their resistance to drought and high temperatures. Such vegetation is not passive in terms of evaporation. Species composition, watering, functional diversity, and exposure conditions determine the ability of plants to survive, to maintain vegetation cover, and to perform the role of evaporation [16, 19, 24]. A photovoltaic module can shelter the plants from overheating during warm seasons, but prolonged shading may impair plant exposure and alter thermal conditions of the substrate. In terms of roof environment, the question is the degree of obstruction that will lower surface heating, but allow the plant layer to act as an exposed living surface.

Photovoltaic generation is an additional driving force of this study. Crystalline photovoltaic modules decrease energy efficiency with the rise in the temperature of cells, and lower roof temperatures and temperature of air nearby increase energy production. Prior roof-comparison studies confirmed the dependence of energy yields from solar cells on thermal conditions of surfaces [20, 26]. Studies focused specifically on integration of photovoltaics into green roofs concluded that vegetation can positively impact temperature and/or energy yield if geometrical factors and climate are favorable [2, 9, 11, 22, 27]. Reviews of integrated photovoltaic-green roof technology also identified several important components: height of the module, plant composition, condition of the substrate, climate, and maintenance [1, 15]. This literature highlights the importance of hydrothermal behavior of vegetation in terms of performance of photovoltaic green roofs.

In this paper, the half-shaded condition of the Ljubljana sedum photovoltaic green roof will be compared against complete exposure and complete obstruction in relation to daily agreement between measured and modelled evapotranspiration, temperature response of the vegetation, long-wave correction of evapotranspiration, and soil heat-flux fraction. The comparison is made with the help of the Hydrothermal Constraint Number. Results will be used for the initial evaluation of layout of a module and will allow to optimize module placement (clearance, row spacing, tilt, coverage).

2. Materials and Methods

2.1. Roof configuration and shade states

The analysis utilizes measured data from a monitored extensive roof covered with sedum and photovoltaic modules installed in Ljubljana [29]. The studied roof has typical characteristics of an extensive roof: planted layer, mineral-organic substrate, drainage layer, waterproof roof membrane, and metal module frame above the vegetation layer. The module partly blocks incoming direct solar radiation and changes long-wave conditions above the canopy. Data required for calculation include the daily values of evapotranspiration, their uncertainty, coefficients describing the response of vegetation surface temperature to radiation, and daily fractions of soil heat flux under three different shades.

The data included in Table 1 can be viewed as a concise set of related roof measurements and constants. The paired values for evapotranspiration per day establish a balance of the water budget, the equation for the temperature determines the thermal response to shading, the correction for the longwave radiation corresponds to the radiation penalty imposed by the module, and the shares of soil heat fluxes correspond to the three observed states of shading. Thus, the table does not just include input values but also indicates what component of the roof process each value affects.

Table 1. Roof quantities used in the calculation.

Quantity	Values	Role in the calculation
Evapotranspiration reference dates	9 July, 25 July, and 3 August 2024	Tests whether the daily water-balance values are sufficiently consistent for comparative ranking
Vegetation temperature relation	$\theta_v = 0.935\theta_a + 0.011 R_g(1 - S)$	Converts module shade into a reduction in the solar component of vegetation temperature
Longwave omission	0.51 mm day^{-1} relative to 2.93 mm day^{-1}	Represents the evapotranspiration error caused by excluding photovoltaic longwave exchange
Soil heat-flux fractions	0.116, 0.088, and 0.054	Evaluates how close each measured shade state is to the $C^\star = 0.10$ daily reference proportion
Shading states	$S = 0$, $S = 0.5$, and $S = 1$	Defines the directly measured unshaded, half-shaded, and fully shaded states

A schematic representation of the physical roof structure described by the aforementioned quantities can be found in Figure 1. Here, three images illustrate the three distinct states of shading in the style of a roof cross section photograph.

(a) Unshaded surface. **(b)** Half-shaded surface. **(c)** Fully shaded surface.

Figure 1. PV module, sedum, substrate, and drainage layers.

The roof domain shown in Figure 1 explains why the calculations take into account multiple factors and not just the presence of shade. Not only does the module act as a shortwave barrier but also acts as a radiative surface above the plant cover and an obstacle that affects the process of heat fluxes from the substrate. Drainage layer and shallow substrate play a role too because of the limitation in heat capacity and moisture availability caused by the thin structure of the roof assembly. Therefore, such approach of taking into consideration all the factors mentioned previously is justified.

The shading factor, S, equals the percentage of obstruction of the direct solar input at the vegetation surface. Therefore, $S = 0$ means no shading at all, $S = 0.5$ refers to half obstruction of the direct solar input, while $S = 1$ implies full obstruction of the direct solar input. The other values are used only for illustration purposes; however, the Hydrothermal Constraint Number is computed only for the values of S mentioned above.

2.2. Daily evapotranspiration agreement

Daily evapotranspiration fidelity is evaluated from the three reference dates. For each date, the signed difference between modelled and measured daily evapotranspiration is

$$e_i = ET_{\mathrm{mod},i} - ET_{\mathrm{meas},i}. \tag{1}$$

The uncertainty-normalized discrepancy is

$$z_i = \frac{|e_i|}{\sqrt{u_{\mathrm{meas},i}^2 + u_{\mathrm{mod},i}^2}}, \tag{2}$$

where $u_{\mathrm{meas},i}$ and $u_{\mathrm{mod},i}$ are the respective uncertainty values. This form matters because a roof-surface evapotranspiration difference should not be judged only by absolute magnitude. A small numerical difference can still be meaningful if uncertainty is very low, while a slightly larger difference may be acceptable if it falls within the combined uncertainty envelope.

The evapotranspiration agreement term is calculated as

$$F_{ET} = 1 - \frac{\mathrm{RMSE}_{ET}}{\overline{ET}_{\mathrm{meas}}}. \tag{3}$$

This term does not imply universal validity for the roof model. It acts as a reliability control within the HCN calculation. A high value indicates that the daily evapotranspiration evidence is coherent enough to support a ranking of shade states; a low value would reduce the final score even if the thermal and soil heat terms appeared favourable.

2.3. Shade-dependent vegetation temperature

The vegetation surface-temperature relation is

$$\theta_v = 0.935\theta_a + 0.011R_g(1 - S), \tag{4}$$

where θ_v is vegetation surface temperature, θ_a is air temperature, R_g is global solar radiation, and S is direct shade fraction. The coefficient 0.935 indicates strong coupling between vegetation and air temperature in the temperature relation. The coefficient 0.011 gives the temperature change associated with the shade-sensitive solar term.

At a high-sun comparison value of $R_g = 800\,\mathrm{W\,m^{-2}}$, the solar component is

$$\Delta\theta_{\mathrm{solar}}(S) = 0.011R_g(1 - S), \tag{5}$$

while the shade-induced thermal relief relative to the unshaded state is

$$\Delta\theta_{\mathrm{relief}}(S) = 0.011R_gS. \tag{6}$$

These equations give the shade term a direct physical interpretation. Each $100\,\mathrm{W\,m^{-2}}$ reduction in shade-sensitive solar input lowers the solar component of vegetation temperature by about 1.1 °C. The total surface temperature may differ because air temperature, substrate moisture, wind, canopy condition, and longwave exchange also act on the plant surface, but the direct-solar contribution is clearly quantified.

2.4. Hydrothermal Constraint Number calculation

The Hydrothermal Constraint Number combines four terms: soil heat-flux conformance, balanced exposure, longwave-aware evapotranspiration protection, and daily evapotranspiration fidelity. It is calculated as

$$\mathrm{HCN}(S) = w_GB_G(S) + w_SB_S(S) + w_LB_L + w_EF_{ET}, \tag{7}$$

with $w_G = 0.40$, $w_S = 0.30$, $w_L = 0.20$, and $w_E = 0.10$. These weights place the largest emphasis on soil heat-flux conformance, followed by balanced plant exposure, longwave correction, and evapotranspiration fidelity.

The soil heat term is calculated as

$$B_G(S) = 1 - |C_G(S) - C^\star|/C^\star, \tag{8}$$

where $C^\star = 0.10$. The exposure balance term is

$$B_S(S) = 4S(1 - S), \tag{9}$$

which gives its maximum at half direct-solar obstruction and falls to zero at both full sun and full shade. The longwave term is

$$P_L = \frac{0.51}{2.93} = 0.174, \qquad B_L = 1 - P_L = 0.826. \tag{10}$$

The calculation remains deliberately compact because it compares measured shade states before any full-season roof simulation is available. Its value lies in showing why a state that is thermally cooler is not automatically the best hydrothermal state if plant exposure and soil heat partitioning deteriorate.

3. Results

3.1. Daily evapotranspiration agreement

Measured and modelled daily evapotranspiration values are shown in Table 2. The three dates cover two higher evapotranspiration days near 4 mm day^{-1} and one lower day at 2.60 mm day^{-1}, allowing the fidelity term to test both magnitude and proportional error.

Table 2. Daily evapotranspiration agreement.

Date	ET_{meas}	ET_{mod} (mm day^{-1})	Error	z_i	APE (%)
9 July 2024	3.98 ± 0.04	4.15 ± 0.15	+0.17	1.10	4.27
25 July 2024	4.08 ± 0.04	3.95 ± 0.14	-0.13	0.89	3.19
3 August 2024	2.60 ± 0.04	2.73 ± 0.11	+0.13	1.11	5.00

The values in Table 2 show no persistent daily bias. Modelled evapotranspiration is slightly higher than measured evapotranspiration on 9 July and 3 August, but slightly lower on 25 July. The absolute errors remain between 0.13 mm day^{-1} and 0.17 mm day^{-1}. The uncertainty-normalized values, 1.10, 0.89, and 1.11, are close to one, which means that the discrepancies are comparable to the combined uncertainty envelopes rather than being much larger than them.

The root mean square error is 0.145 mm day^{-1}, and the mean measured evapotranspiration is 3.553 mm day^{-1}. The fidelity term is therefore

$$F_{ET} = 1 - \frac{0.145}{3.553} = 0.959. \tag{11}$$

A value of 0.959 is high enough for the daily water-balance evidence to support a comparative hydrothermal score. The interpretation is strongest for the specific roof and reference dates because the evidence is daily and local. It should not be generalized to all sedum roofs without additional measurement, but it is sufficient to keep evapotranspiration reliability from being a weak point in the shade-state comparison.

The visual comparison in Figure 2 places the three daily pairs beside the roof surface. The measured and modelled water-depth columns remain close on all three dates, which visually reinforces the numerical result that the water-balance component is stable relative to the daily magnitudes.

The three-panel comparison in Figure 2 also highlights why daily depth is a useful scale for this paper. A difference of 0.13 mm day^{-1} is small in absolute terms, but it becomes a larger percentage on the lower evapotranspiration day.

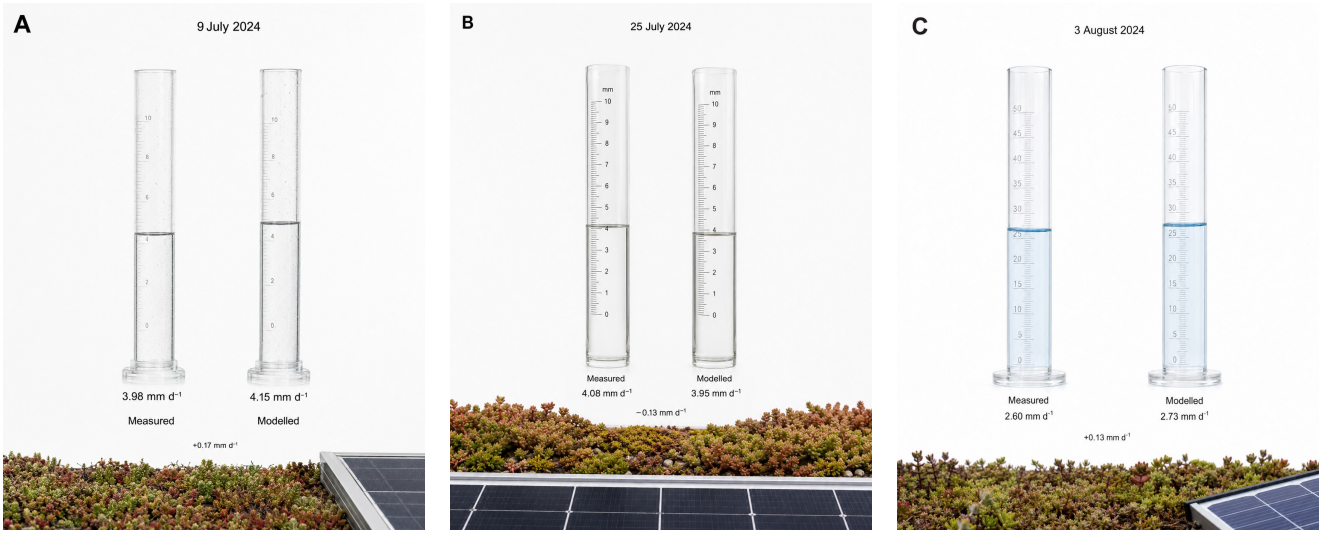

(a) 9 July 2024. **(b)** 25 July 2024. **(c)** 3 August 2024.

Figure 2. Measured and modelled daily evapotranspiration.

Roof irrigation and substrate storage are commonly planned in millimetres of water depth, so repeated small daily errors can accumulate into meaningful differences in plant stress, drainage expectation, or latent-cooling estimation. The fidelity term keeps this uncertainty visible while still allowing the ranking to proceed.

3.2. Vegetation temperature under module obstruction

The temperature coefficients are summarized in Table 3. The intercept is not used because its statistical support was insufficient, while the air-temperature and solar-radiation terms are used in the relation.

Table 3. Vegetation temperature coefficients.

Term	Symbol	Value	Statistical evidence	Interpretation
Intercept	a	excluded	$p = 0.13$	Excluded from the temperature relation
Air temperature	θ_a	0.935	$p < 0.001$	Vegetation surface temperature closely follows air temperature
Solar radiation with shade	$R_g(1 - S)$	0.011	$p < 0.001$	Direct-solar input raises the vegetation temperature component

The coefficients in Table 3 separate the atmospheric and module-controlled parts of the temperature relation. Air temperature remains the dominant background condition, but the solar coefficient is the design-sensitive term because row spacing, module height, module tilt, and coverage ratio all affect S. This makes the temperature equation useful for layout comparison while preserving the HCN calculation.

Table 4. Shade-dose temperature response at $R_g = 800\,\mathrm{W\,m^{-2}}$.

Shade fraction S	Solar component (°C)	Thermal relief	Balanced exposure B_S
0.0	8.80	0.00	0.00
0.3	6.16	2.64	0.84
0.5	4.40	4.40	1.00
0.8	1.76	7.04	0.64
1.0	0.00	8.80	0.00

The values in Table 4 demonstrate the difference between thermal relief and hydrothermal suitability. Complete

shade removes the direct-solar temperature component, but its balanced exposure score is zero. No shade preserves full plant exposure, but it provides no solar thermal relief and also has a balanced exposure score of zero. The half-shaded state sits at the centre of the exposure function, with $B_S = 1.00$, and removes 4.40 °C from the direct-solar component at $R_g = 800\,\mathrm{W\,m^{-2}}$. The temperature calculation therefore supports partial shade not because it is the coolest state, but because it is the state that keeps the direct-solar term and the shade relief in balance.

The field appearance of the shade-dose states is shown in Figure 3. The images are intentionally photographic rather than diagrammatic because the important design condition is the material exposure of the sedum surface under an actual module edge.

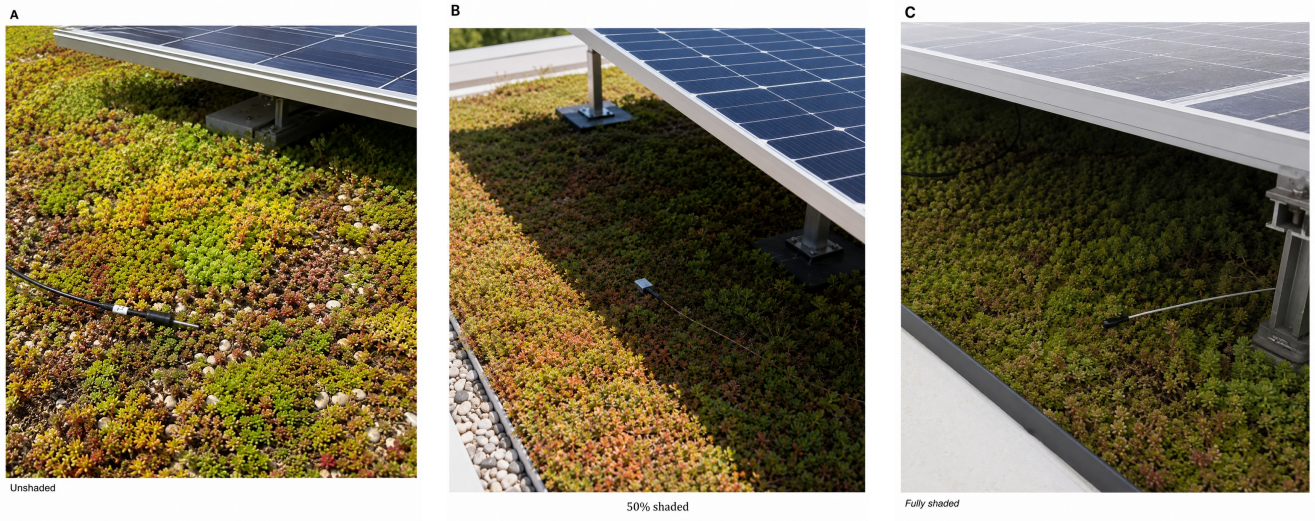

(a) Open sedum. **(b)** Module-edge shade. **(c)** Deep shade.

Figure 3. Shade-dose exposure states.

The roof views in Figure 3 show the physical transition behind Eq. (5). Partial shade is not a numerical midpoint only. It is a plant-surface condition in which some sedum remains exposed while another portion is protected by the module. This matters because plant cover, substrate moisture, and sensor response are all spatially affected by the edge of the panel. A layout that produces a moving or broken shade band can therefore differ from a layout that creates persistent deep shade, even if both have similar average obstruction at one instant.

3.3. Soil heat flux and longwave evapotranspiration

The hydrothermal score uses the daytime soil heat-flux fraction of how close each shade state remains to the daily reference proportion $C^\star = 0.10$. The measured fractions are 0.116 for the unshaded state, 0.088 for the half-shaded state, and 0.054 for the fully shaded state. Their corresponding conformance scores are 0.84, 0.88, and 0.54.

The sensing context in Figure 4 shows the sedum and substrate exposure associated with these states. Although the images do not measure heat flux by themselves, they help the reader understand why the same roof assembly can produce different substrate heat partitioning under different module obstruction.

The progression in Figure 4 gives a material explanation for the soil heat result. The unshaded roof receives strong direct radiation and has a soil heat-flux fraction slightly above the reference. The half-shaded state is closest to the target value, which suggests that moderate obstruction reduces excessive solar forcing without suppressing substrate heat exchange too strongly. The fully shaded state has the weakest conformance because the soil heat-flux fraction falls to 0.054, well below the reference value. This confirms that maximum shade is not automatically a stable hydrothermal condition for a shallow sedum roof.

The longwave component is summarized in Table 5. Omitting photovoltaic longwave exchange produces a daily evapotranspiration difference of 0.51 mm day^{-1} relative to a detailed daily estimate of 2.93 mm day^{-1}. The

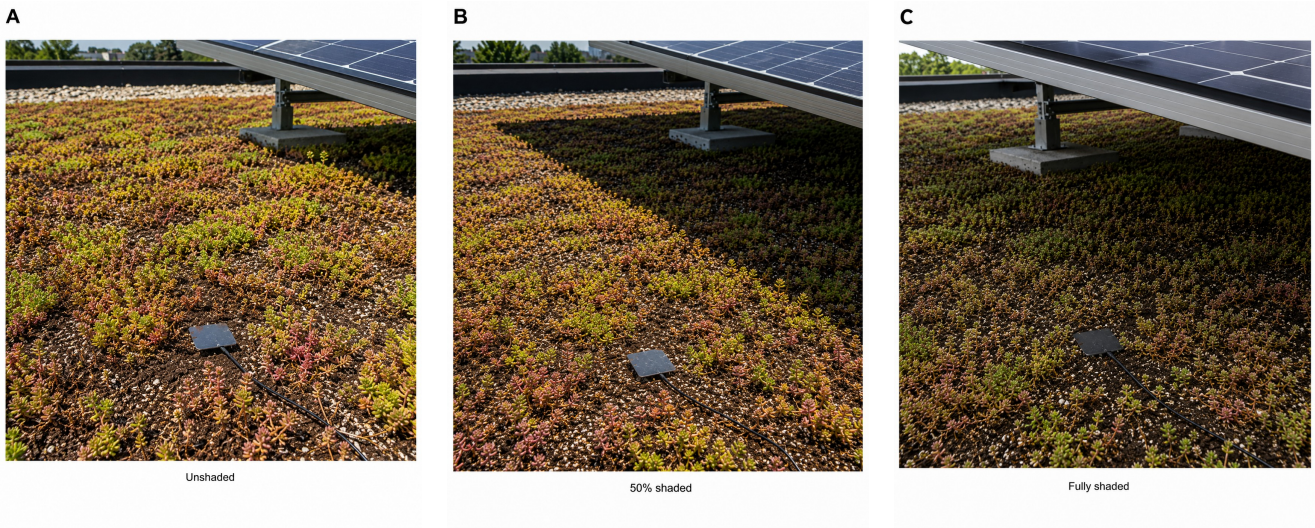

(a) Unshaded. **(b)** Half shaded. **(c)** Fully shaded.

Figure 4. Sedum surface and heat-flux sensing context.

proportional penalty is therefore 0.174, leaving $B_L = 0.826$.

Table 5. Longwave evapotranspiration correction.

Quantity	Value	Unit or meaning
Detailed daily evapotranspiration	2.93	$\mathrm{mm\,day^{-1}}$
Omitted longwave contribution	0.51	$\mathrm{mm\,day^{-1}}$
Proportional penalty P_L	0.174	fraction of detailed ET
Remaining balance B_L	0.826	longwave-aware term
Water volume over 100 $\mathrm{m^2}$	51	$\mathrm{L\,day^{-1}}$
Water volume over 500 $\mathrm{m^2}$	255	$\mathrm{L\,day^{-1}}$

The numbers in Table 5 show why longwave exchange cannot be dismissed as a minor radiative detail. A depth of 0.51 $\mathrm{mm\,day^{-1}}$ equals 0.51 $\mathrm{L\,m^{-2}\,day^{-1}}$. Over even a modest roof area, the difference becomes a meaningful water volume. If the same omission persisted during a dry sequence, irrigation demand, substrate storage interpretation, and latent-cooling estimates would all be biased downward.

The scale of this penalty is translated into roof-surface terms in Figure 5. The panels connect the module-covered sedum surface with the water-depth and roof-area quantities used in the calculation.

The visual evidence in Figure 5 is important because water-balance errors are often difficult to interpret from millimetres alone. The conversion to 51 $\mathrm{L\,day^{-1}}$ over 100 $\mathrm{m^2}$ and 255 $\mathrm{L\,day^{-1}}$ over 500 $\mathrm{m^2}$ shows that the radiative environment beneath modules has operational consequences. Longwave exchange affects not only an equation term but also irrigation scheduling, interpretation of substrate drying, and the estimate of cooling supplied by latent heat flux.

3.4. Hydrothermal ranking of shade states

The Hydrothermal Constraint Number for the three measured shade states is given in Table 6. The half-shaded state obtains the highest score, 0.913. The unshaded state obtains 0.597, and the fully shaded state obtains 0.477.

The ranking in Table 6 is not a marginal preference. The half-shaded state exceeds the unshaded state by 0.316 HCN units and the fully shaded state by 0.436 HCN units. The common contribution from longwave protection and evapotranspiration fidelity is identical across the three measured states: $0.20 \times 0.826 + 0.10 \times 0.959 = 0.261$. The

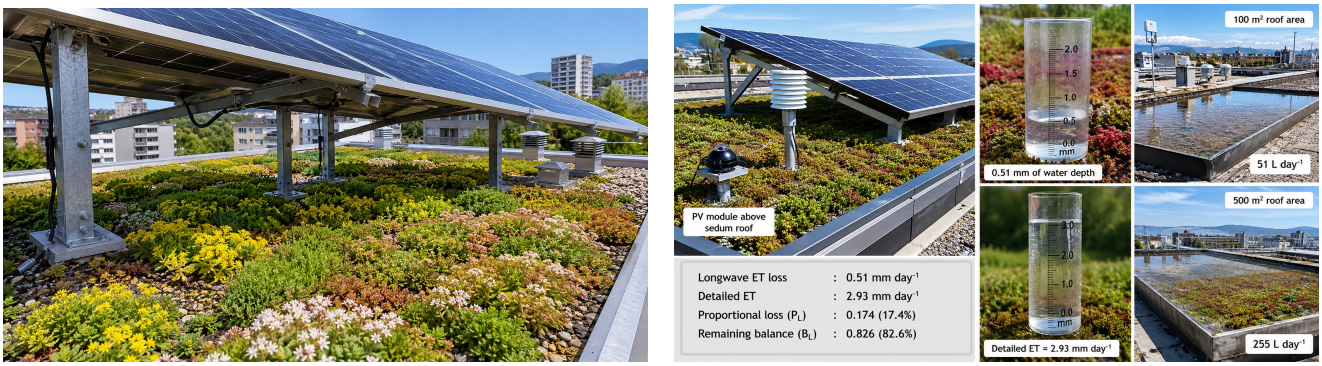

(a) Module over sedum.

(b) Water-depth equivalent.

(c) Roof volume.

(d) Shaded sedum.

Figure 5. Longwave water-depth and roof-volume context.

Table 6. Hydrothermal Constraint Number by shade state.

State	S	C_G	B_G	B_S	HCN
Unshaded	0.0	0.116	0.84	0.00	0.597
Half shaded	0.5	0.088	0.88	1.00	0.913
Fully shaded	1.0	0.054	0.54	0.00	0.477

difference is therefore governed by soil heat conformance and balanced exposure. The half-shaded state performs best because it has both the highest soil heat-flux conformance and the only maximum balanced-exposure score.

The roof-scale sequence in Figure 6 provides a visual counterpart to the ranking. It shows how the measured shade states occupy different parts of the module-covered vegetated surface.

The strip in Figure 6 helps distinguish the three score outcomes. The unshaded state has strong plant exposure and a reasonable soil heat-flux fraction, but it leaves the full direct-solar temperature component in place. The fully shaded state gives the strongest solar thermal relief, but it removes balanced exposure and shifts the soil heat-flux fraction too far below the reference. The half-shaded state is the only measured condition that reduces solar heating while preserving a favourable substrate heat partition. The HCN therefore does not simply reward shade; it rewards the state where shade, exposure, and soil heat share are jointly credible.

3.5. Weight response and roof operation

The weights emphasize hydrothermal stability, but the ranking does not depend on treating them as universal constants. The half-shaded state dominates the balanced exposure term and also has the highest soil heat conformance. Moderate changes to w_G or w_S would therefore not remove its advantage unless the comparison were deliberately

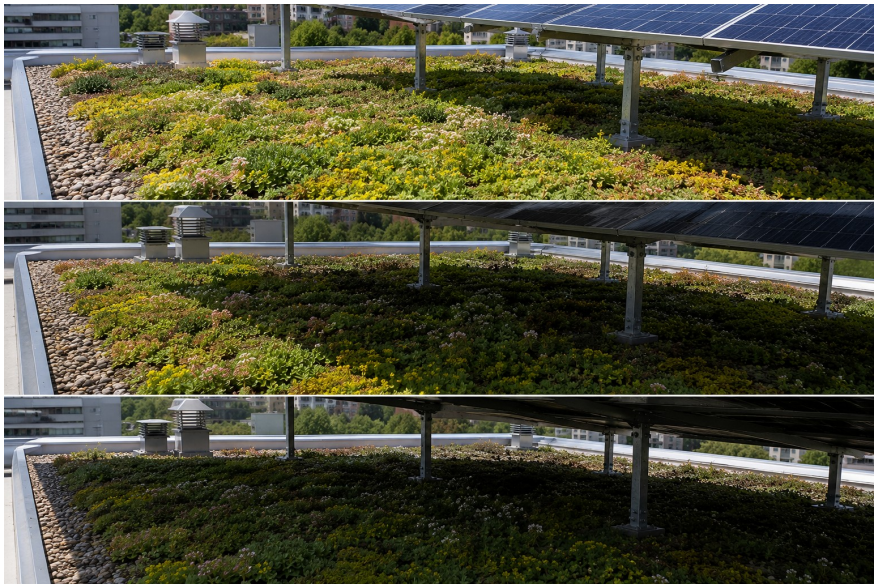

Figure 6. Supported shade-state sequence.

changed to ignore plant exposure or ignore soil heat partitioning. A design that assigned nearly all importance to direct solar temperature relief would favour full shade. A design that assigned nearly all importance to open plant exposure would favour no shade. The HCN separates those extremes by placing exposure and soil heat partitioning in the same calculation.

The operating interpretation is shown in Figure 7. The panels present the roof states as field-like conditions rather than as abstract categories.

The operating views in Figure 7 show why the result is relevant to module layout. A designer can create partial obstruction through row spacing, tilt angle, clearance, and orientation. The same HCN result does not prescribe one geomeasure solution, but it indicates the hydrothermal target: avoid leaving the sedum roof fully exposed during high solar load, and avoid covering it so completely that direct plant exposure and soil heat partitioning are suppressed. The preferred state is a roof surface with moderated direct-solar forcing and vegetation function.

The hydrological observation context is shown in Figure 8. This view connects the evapotranspiration calculation with the actual roof environment in which water depth, module coverage, sedum cover, and substrate condition are observed together.

Roof Setting (Figure 8) highlights the relevance of the interpretation of evapotranspiration as a surface-level phenomenon as opposed to its presentation in purely numerical form. The rain-gauge setting, sedum coverage, adjacent modules, gravel margin, and urban roof placement are parts of a single hydrology environment. This is why daily values are used to justify the particular roof state, and transfer of the score to another roof implies the consideration of climate, substrate, vegetation, irrigation, module layout, and measurement methods.

(a) Rooftop state sequence.

(b) Module-shade roof bays.

Figure 7. Operational shade states.

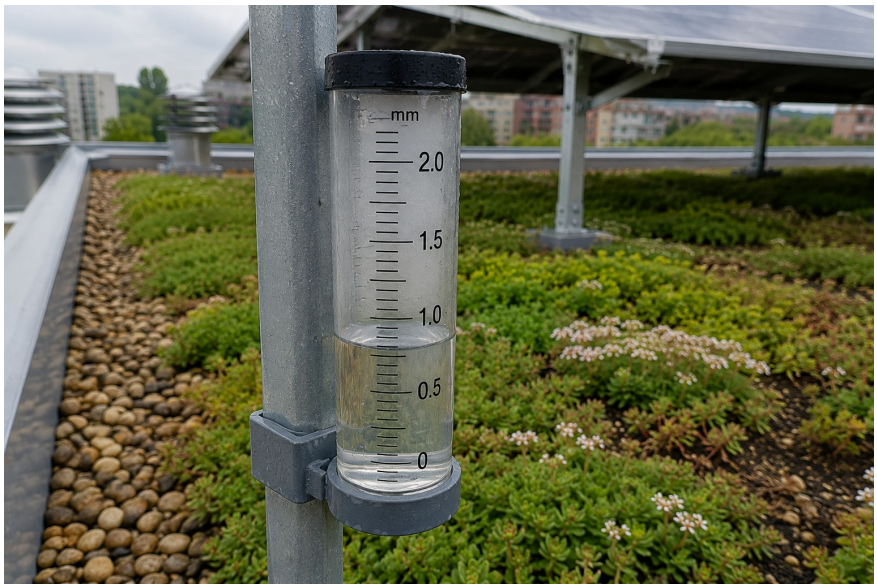

Figure 8. Roof-surface hydrological observation setting.

4. Discussion

As seen from the results, the half-shaded state is the strongest roof hydrothermal operating state compared with full exposure and complete shading states. The reasoning does not follow from the position that half shade stands halfway between full exposure and complete shading. Rather, the result is explained by the interaction of four

quantified terms: strong evapotranspiration agreement allows the direct comparison; the vegetation temperature relationship gives a direct-solar relief of 4.40 °C at $S = 0.5$ and $R_g = 800\,\mathrm{W\,m^{-2}}$; longwave penalty is significant enough to affect interpretation of water balance on a roof; and the soil heat-flux share under the half-shaded state is close to the 10 % reference value. Combined, these components provide explanation for how HCN = 0.913 is achieved in case of $S = 0.5$ whereas the other two states yield scores of 0.597 and 0.477.

These conclusions coincide with existing green roof energy and hydrology literature and allow giving photovoltaic green roof interpretation based on the measurements carried out in Ljubljana. Green roofs rely on the joint dynamics of heat and moisture within plant layer and substrate cover [13, 25, 28]. Photovoltaic modules cause change in radiation field above the plants. Fully shaded state, thus, cannot be considered the preferred state only due to its reduced direct-solar heating capacity. Although the completely shaded state removes the solar component of vegetation temperature, it also causes the low soil heat-flux fraction of $C_G = 0.054$, which is much lower than the reference one, and no balanced direct solar exposure of vegetation. Moreover, plant-ecological literature also provides examples proving that green roof vegetation performance depends on moisture, substrate, exposure, and biodiversity rather than thermal protection only [16, 19].

The water balance outcome is significant from a practical point of view as roof water depths are low. Despite the evapotranspiration RMSE is $0.145\,\mathrm{mm\,day^{-1}}$ (which seems insignificant in comparison with daily amounts), the depth of just several millimetres determines substrate drying, irrigation requirements, and latent cooling. Reviews of green roofs hydrological literature prove their high sensitivity to antecedent moisture, rainfall pattern, substrate parameters, and vegetation state [5, 17]. The normalization of discrepancy by the value of uncertainty is close to one in the measured states and does not exceed it. Hence, the use of $F_{ET} = 0.959$ as the water-balance reliability term is justified.

The inclusion of the longwave penalty affects roof-shade interpretation. Shade effect is normally considered only as an impact on short-wave radiation. The omission of the longwave correction by $0.51\,\mathrm{mm\,day^{-1}}$ compared with $2.93\,\mathrm{mm\,day^{-1}}$ (i.e., 17.4%) is a relevant parameter for photovoltaic green roofs. Previously conducted energy-related experiments demonstrated the role of photovoltaic, roof reflectivity, and vegetation in affecting sensible heat flux and energy balance of a roof [8, 26]. In the studied roof, the omission of the longwave term changes the estimated daily evapotranspiration amount.

In turn, the decomposition helps to understand the ranking order in the HCN. In fact, the score is composed of common longwave protection (26.1) and evapotranspiration agreement (31.5) terms and differentiating terms of 0.336, 0.652, and 0.216 for unshaded, half-shaded, and fully shaded states, correspondingly. This means that the half-shaded state is better due to the matching directions of the adjustable roof factors. This information is more valuable than simply reporting HCN as a resulting number and allows concluding that the shade level should keep plant surface partially exposed.

Of course, one cannot interpret this result as the rule of thumb implying that 50% shade is the optimal one in every roof configuration. Depending on the climate, plant type, substrate depth, irrigation, wind, module clearance, and season, the optimal solar angle will vary. A Mediterranean roof, a humid temperate roof, and an irrigated semi-arid roof will have different moisture limits and advantages of module shading [6, 9, 10]. However, this general conclusion can be made: if daily evapotranspiration agreement is high, the solar temperature coefficient is applicable, the longwave penalty is considerable, and soil heat-flux shares differ for shade states, the intermediate state is preferable as it conforms to all of the specified conditions simultaneously.

Photographs provide a good link between calculation and roof settings. Cutaway illustration highlights layers where heat and moisture are moving. Figures demonstrating evapotranspiration show close agreement of daily water depths in the states on selected dates. Shade-dose photographs show exposure gradient caused by the edge of the modules. Images of heat fluxes show sedum and substrate surfaces corresponding to the soil heat-flux states. The longwave-water graph illustrates the translation of radiation term into water volumes. Operating-state photos return the numerical ranking to the physical roof setting. The equations, tables, and surfaces are analyzed together as complementary data sources.

Calculation limitations have been discussed before, but it is worth emphasizing them again. They include using

daily values for evapotranspiration, temperature, and radiation rather than a time-resolved one. Soil heat-flux fractions are known for three states; therefore, HCN is not calculated as a function of S. The temperature coefficient cannot be extrapolated outside the roof and current meteorological conditions. Longwave penalty term is included in a daily manner and is not differentiated by time or module temperature. Hydrothermal score does not consider photovoltaic yield, physiological response of plants, substrate drainage hysteresis, snow, long-term cover of plants, maintenance access, and soiling. The restrictions ensure focus of the analysis on hydrothermal behavior.

Next applications of this approach require measurements of radiation, temperature, moisture, and soil heat fluxes as a function of time in order to test whether the intermediate-shaded state is still the best one. More specifically, the calculation can be modified by replacing S with $S(t)$, aggregation of HCN in the relevant part of the day. Additionally, the effect of species-specific plant response and electricity yield of photovoltaic modules can be taken into account in subsequent comparisons. The inclusion of additional factors would increase future analysis, but they are unnecessary at this moment due to the sufficient amount of evidence provided by the Ljubljana measurements. Therefore, it is safe to conclude that partial shading by the photovoltaic module is the strongest hydrothermal roof operating state.

5. Conclusion

Among three roof states with full exposure, partial shading, and complete direct solar obstruction, the latter one is the strongest hydrothermal state. The half-shaded state achieves the highest value of HCN = 0.913 as compared with 0.597 and 0.477 obtained for the other two roof states.

Such a conclusion can be drawn due to combined effects rather than shade preference. The three reference dates showed high evapotranspiration agreement (0.145 mm day^{-1} RMSE and 4.15 % MAPE); the vegetation temperature relationship gave direct-solar relief of 4.40 °C at R_g = 800 W m^{-2}; the omission of the longwave correction is meaningful and corresponds to 51 liters of water per 100 m^2; the soil heat-flux fraction 0.088 is the closest to the reference of 0.10.

It must be noted that the best hydrothermal state is neither a completely shaded state nor full exposure. Rather, it is the measured half-shaded state, where the modules reduce direct-solar heating but preserve plant exposure and do not significantly deviate the soil heat-flux share from the reference value. The implication for early photovoltaic green roof layout includes proper clearance, row spacing, inclination, and coverage to give partial shading. Transfer to another roof will also involve the same set of criteria but adjusted for the specific roof and climate conditions.

References

[1] Abdalazeem, M. E., Hassan, H., Asawa, T., & Mahmoud, H. (2022). Review on integrated photovoltaic-green roof solutions on urban and energy-efficient buildings in hot climate. Sustainable Cities and Society, 82, 103919.

[2] Alshayeb, M. J., & Chang, J. D. (2018). Variations of PV panel performance installed over a vegetated roof and a conventional black roof. Energies, 11(5), 1110.

[3] Allen, R. G., Pereira, L. S., Raes, D., & Smith, M. (1998). Crop evapotranspiration-Guidelines for computing crop water requirements-FAO Irrigation and drainage paper 56. Fao, rome, 300(9), D05109.

[4] Berardi, U., GhaffarianHoseini, A., & GhaffarianHoseini, A. (2014). State-of-the-art analysis of the environmental benefits of green roofs. Applied energy, 115, 411-428.

[5] Berndtsson, J. C. (2010). Green roof performance towards management of runoff water quantity and quality: A review. Ecological engineering, 36(4), 351-360.

[6] Bevilacqua, P., Bruno, R., & Arcuri, N. (2020). Green roofs in a Mediterranean climate: Energy performances based on in-situ experimental data. Renewable Energy, 152, 1414-1430.

[7] Castleton, H. F., Stovin, V., Beck, S. B., & Davison, J. B. (2010). Green roofs; building energy savings and the potential for retrofit. Energy and buildings, 42(10), 1582-1591.

[8] Cavadini, G. B., & Cook, L. M. (2021). Green and cool roof choices integrated into rooftop solar energy modelling. Applied Energy, 296, 117082.

[9] Chemisana, D., & Lamnatou, C. (2014). Photovoltaic-green roofs: An experimental evaluation of system performance. Applied Energy, 119, 246-256.

[10] Feng, Y., Burian, S. J., & Pardyjak, E. R. (2018). Observation and estimation of evapotranspiration from an irrigated green roof in a rain-scarce environment. Water, 10(3), 262.

[11] Fleck, R., Gill, R., Pettit, T. J., Torpy, F. R., & Irga, P. J. (2022). Bio-solar green roofs increase solar energy output: The sunny side of integrating sustainable technologies. Building and Environment, 226, 109703.

[12] Getter, K. L., & Rowe, D. B. (2006). The role of extensive green roofs in sustainable development. HortScience, 41(5), 1276-1285.

[13] Jaffal, I., Ouldboukhitine, S. E., & Belarbi, R. (2012). A comprehensive study of the impact of green roofs on building energy performance. Renewable energy, 43, 157-164.

[14] Jahanfar, A., Drake, J., Gharabaghi, B., & Sleep, B. (2020). An experimental and modeling study of evapotranspiration from integrated green roof photovoltaic systems. Ecological Engineering, 152, 105767.

[15] Lamnatou, C., & Chemisana, D. (2015). A critical analysis of factors affecting photovoltaic-green roof performance. Renewable and Sustainable Energy Reviews, 43, 264-280.

[16] Lundholm, J., MacIvor, J. S., MacDougall, Z., & Ranalli, M. (2010). Plant species and functional group combinations affect green roof ecosystem functions. PloS one, 5(3), e9677.

[17] Mentens, J., Raes, D., & Hermy, M. (2006). Green roofs as a tool for solving the rainwater runoff problem in the urbanized 21st century?. Landscape and urban planning, 77(3), 217-226.

[18] Monteith, J. L. (1965). Evaporation and environment.

[19] Nagase, A., & Dunnett, N. (2010). Drought tolerance in different vegetation types for extensive green roofs: Effects of watering and diversity. Landscape and urban planning, 97(4), 318-327.

[20] Nagengast, A., Hendrickson, C., & Matthews, H. S. (2013). Variations in photovoltaic performance due to climate and low-slope roof choice. Energy and Buildings, 64, 493-502.

[21] Oberndorfer, E., Lundholm, J., Bass, B., Coffman, R. R., Doshi, H., Dunnett, N., ... & Rowe, B. (2007). Green roofs as urban ecosystems: ecological structures, functions, and services. BioScience, 57(10), 823-833.

[22] Ogaili, H., & Sailor, D. J. (2016). Measuring the effect of vegetated roofs on the performance of photovoltaic panels in a combined system. Journal of Solar Energy Engineering, 138(6), 061009.

[23] Penman, H. L. (1948). Natural evaporation from open water, bare soil and grass. Proceedings of the Royal Society of London. Series A. Mathematical and Physical Sciences, 193(1032), 120-145.

[24] Rowe, D. B. (2011). Green roofs as a means of pollution abatement. Environmental pollution, 159(8-9), 2100-2110.

[25] Sailor, D. J. (2008). A green roof model for building energy simulation programs. Energy and buildings, 40(8), 1466-1478.

[26] Scherba, A., Sailor, D. J., Rosenstiel, T. N., & Wamser, C. C. (2011). Modeling impacts of roof reflectivity, integrated photovoltaic panels and green roof systems on sensible heat flux into the urban environment. Building and Environment, 46(12), 2542-2551. https://doi.org/10.1016/j.buildenv.2011.06.012.

[27] Shafique, M., Luo, X., & Zuo, J. (2020). Photovoltaic-green roofs: A review of benefits, limitations, and trends. Solar Energy, 202, 485-497.

[28] Voyde, E., Fassman, E., Simcock, R., & Wells, J. (2010). Quantifying evapotranspiration rates for New Zealand green roofs. Journal of hydrologic engineering, 15(6), 395-403.

[29] Jahanfar, A., Drake, J., Gharabaghi, B., & Sleep, B. (2020). An experimental and modeling study of evapotranspiration from integrated green roof photovoltaic systems. Ecological Engineering, 152, 105767..